Available online at www.sciencedirect.com

jmr&t Journal of Materials Research and Technology

www.jmrt.com.br

Original Article

Numerical modeling of the dispersion of ceramic nanoparticles during ultrasonic processing of aluminum-based nanocomposites☆

*Daojie Zhang, Laurentiu Nastac**

Department of Metallurgical and Materials Engineering, University of Alabama, Tuscaloosa, United States

ARTICLE INFO

Article history:
Received 10 May 2014
Accepted 22 September 2014
Available online 25 October 2014

Keywords:
Metal–matrix-nano-composites
Ultrasonic processing
Modeling of ceramic nanoparticle dispersion
Aluminum alloys

ABSTRACT

The metal–matrix-nano-composites (MMNCs) in this study consist of a 6061 alloy matrix reinforced with 1.0 wt.% SiC nanoparticles that are dispersed within the matrix using an ultrasonic cavitation dispersion technique available in the Solidification Laboratory at the University of Alabama.

The required ultrasonic parameters to achieve (i) the required stirring and cavitation for suitable degassing and refining of the aluminum alloy and (ii) the adequate fluid flow characteristics for uniform dispersion of the nanoparticles into the 6061 matrix are being investigated in this study by using an in-house developed CFD ultrasonic cavitation model. The multiphase CFD model accounts for turbulent fluid flow, heat transfer, and the complex interaction between the molten alloy and nanoparticles by using the ANSYS's Fluent DDPM.

The modeling parametric study includes the effects of the fluid flow, the ultrasonic probe location, nanoparticle size distribution, and initial location where the nanoparticles are released into the molten alloy. It was determined that the nanoparticles can be distributed quickly and uniformly into the molten 6061 alloy.

1. Introduction

Aluminum-based metal matrix composites (MMCs) have been extensively studied and widely used in the aerospace, automotive and military industries due to their high strength-to-weight ratios and enhanced mechanical and thermal properties including specific modulus, superior strength, stiffness, good wear resistance, fatigue resistance and improved thermal stability [1–3]. However, the particles commonly used are micron-sized which has a counterpart that the ductility of the MMCs deteriorates with high ceramic

☆ Paper presented in the form of an abstract as part of the proceedings of the Pan American Materials Conference, São Paulo, Brazil, July 21st to 25th 2014.

* *Corresponding author.*
E-mail: lnastac@eng.ua.edu (L. Nastac).

http://dx.doi.org/10.1016/j.jmrt.2014.09.001

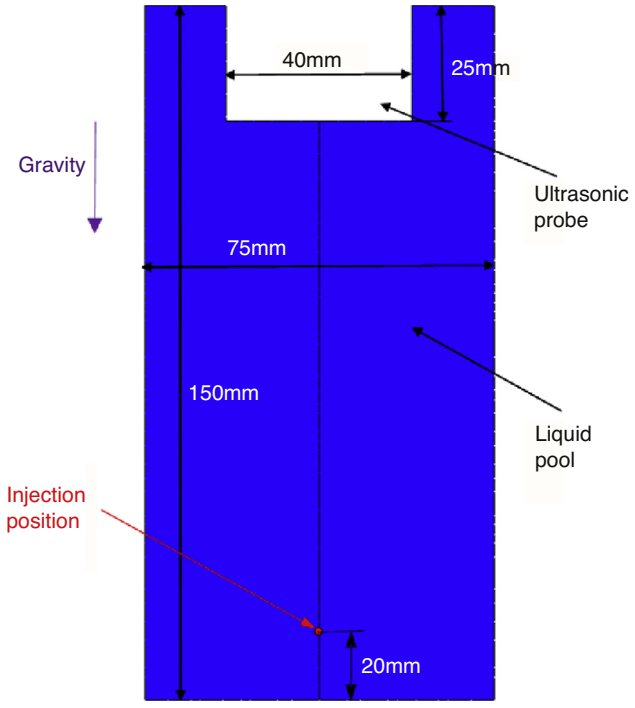

Fig. 1 – Geometry model.

particle concentration [4]. Consequently, more attention has been drawn to metal matrix nanocomposites (MMNCs), since the properties of metallic alloys reinforced by ceramic nanoparticles (with dimensions less than 100 nm) would be enhanced considerably while the ductility of the matrix is retained [5–12].

However, it is extremely difficult to obtain uniform dispersion of nano-sized ceramic particles in liquid metals due to high viscosity, poor wettability in the metal matrix, and a large surface-to-volume ratio, which results in agglomeration and clustering [4]. Currently, several fabrication technologies including high-energy ball milling [9,12], in situ synthesis [8], electroplating [13], and ultrasonic technology (UST) [4–6] are most commonly used, among which UST is supposed to be more reliable and cost effective.

Ansys's Fluent Dense Discrete Phase Model (DDPM) [14] was adapted in this study. The DDPM accounts for turbulent fluid flow, heat transfer, and the complex interaction between the molten alloy and nanoparticles. The dispersion of SiC nanoparticles with different injection positions and probe locations were investigated in detail.

2. Model description

The geometry of the model is shown in Fig. 1. The ultrasonic probe has a diameter of 40 mm. The liquid aluminum is A6061. It has a density of 2700 kg/m^3 and a viscosity of 1.0×10^{-3} kg/(ms). The SiC nanoparticles with an average particle size of 55 nm and density of 3216 kg/m^3 are treated as inert-particles. The mass flow rate of the SiC nanoparticles is 0.014 kg/s. Thus, 1.0 wt.% of SiC nanoparticles can be injected at about 20 mm above the bottom of the furnace for 1 s.

The multiphase computational fluid dynamics (CFD) model accounts for turbulent fluid flow, heat transfer, and the complex interaction between the molten alloy and nanoparticles by using the ANSYS Fluent DDPM and $k-\omega$ turbulence model [14]. The CFD model is described in detail below.

2.1. Fluid flow model

In the Eulerian DDPM multiphase model an Eulerian treatment is used for each phase, and the discrete phase (nanoparticles) is designated as a granular phase. The volume fraction of the particulate phase is accounted for in the conservation equations.

The continuity equation for the phase q is

$$\frac{\partial}{\partial t}(a_q\rho_q) + \nabla\cdot(a_q\rho_q\mathbf{u}_q) = \dot{m}_{pq} - \dot{m}_{qp} \tag{1}$$

The momentum balance for the phase q yields

$$\frac{\partial}{\partial t}(a_q\rho_q\mathbf{u}_q) + \nabla\cdot(a_q\rho_q\mathbf{u}_q\mathbf{u}_q) = -a_q\nabla P + \nabla\cdot[a_q\mu_q(\nabla\mathbf{u}_q + \nabla\mathbf{u}_q^T)] + a_q\rho_q g + \mathbf{f}_{DPM} + \mathbf{f}_{other} \tag{2}$$

where a_q is the phase volume fraction, ρ_q is the density, $\mathbf{u}_q$ is the velocity, μ_q is the molecular viscosity, and P is the pressure shared by all phases. $\dot{m}_{pq}$ characterizes the mass transfer from the pth to qth phase, and $\dot{m}_{qp}$ characterizes the mass transfer from phase q to phase p. The momentum exchange term, $\mathbf{f}_{DPM}$, is considered only in the primary phase equations. The source term, $\mathbf{f}_{other}$, includes the virtual mass force, lift force, turbulent dispersion force, etc.

Eqs. (1) and (2) do not solve for the velocity field and volume fraction of the discrete phase. Their values are obtained from the Lagrangian tracking solution.

2.2. Particle tracking model

The trajectory of a discrete phase particle is predicted by integrating the force balance on the particle. The force balance equates the particle inertia with the forces acting on the particle, and can be written as

$$\frac{d\mathbf{u}_p}{dt} = \mathbf{F}_D + \mathbf{F}_G + \mathbf{F}_B + \mathbf{F}_{virtual\text{-}mass} + \mathbf{F}_{pressure\text{-}gradient} + \mathbf{F}_{lift} + \mathbf{F}_{interaction} \tag{3}$$

where $\mathbf{u}_p$ is the particle velocity, and all the terms at the right-hand are with a unit of force/unit particle mass.

The drag force, $\mathbf{F}_D$, exerted on the particle by the viscous liquid tends to make it follow the fluid flow, and is calculated by

$$\mathbf{F}_D = \frac{18\mu}{\rho_p d_p^2}\frac{C_D\,Re}{24}(\mathbf{u} - \mathbf{u}_p) \tag{4}$$

where $\mathbf{u}$ is the fluid phase velocity, ρ_p is the density of the particle, and d_p is the particle diameter. Re is the relative Reynolds number, which is defined as

$$Re = \frac{\rho d_p \left|\mathbf{u} - \mathbf{u}_p\right|}{\mu} \tag{5}$$

where ρ is the fluid density.

C_D is the drag coefficient which is calculated by the model of Wen and Yu:

$$C_D = \frac{24}{Re}(1 + 0.15Re^{0.687}) \tag{6}$$

The net effect of the buoyancy force, $\mathbf{F}_B$, and the gravitational force, $\mathbf{F}_G$, is

$$\mathbf{F}_G + \mathbf{F}_B = \frac{g(\rho_p - \rho)}{\rho_p} \tag{7}$$

The virtual mass force, $\mathbf{F}_{virtual\text{-}mass}$, is an unsteady force due to a change of the relative velocity of the particle submerged in the fluid, and can be calculated as

$$\mathbf{F}_{virtual\text{-}mass} = \frac{1}{2}\frac{\rho}{\rho_p}\frac{d}{dt}(\mathbf{u} - \mathbf{u}_p) \tag{8}$$

An additional force arises due to the pressure gradient in the fluid:

$$\mathbf{F}_{pressure\text{-}gradient} = \left(\frac{\rho}{\rho_p}\right)\mathbf{u}_p \nabla \mathbf{u} \tag{9}$$

The Saffman's lift force due to shear is generated by the local velocity gradients across the particle, and is calculated as

$$\mathbf{F}_{lift} = \frac{2Kv^{1/2}\rho d_{ij}}{\rho_p d_p (d_{lk} d_{kl})^{1/4}}(\mathbf{u} - \mathbf{u}_p) \tag{10}$$

where $K = 2.594$ and d_{ij} is the deformation tensor.

The term, $\mathbf{F}_{interaction}$, models the additional acceleration acting on a particle, resulting from interparticle interaction. It is computed from the stress tensor given by the Kinetic Theory of Granular Flows as

$$\mathbf{F}_{interaction} = -\frac{1}{\rho_p}\nabla \cdot \bar{\bar{\tau}}_s \tag{11}$$

where $\bar{\bar{\tau}}_s$ is the stress-strain tensor of the granular phase.

The chaotic effect of turbulence on the particle trajectories is accounted for using the stochastic tracking approach, i.e., the discrete random walk (DRW) model:

$$\mathbf{u} = \bar{\mathbf{u}} + \zeta\sqrt{\frac{2k}{3}} \tag{12}$$

where $\bar{\mathbf{u}}$ is the mean fluid velocity in the trajectory Eq. (3), ζ is a normally distributed random number, and k is the local turbulent kinetic energy.

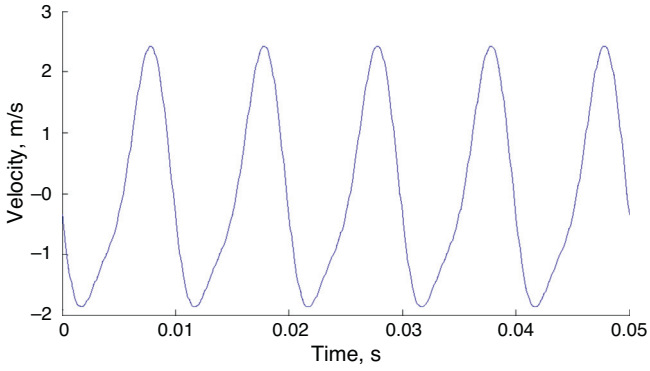

Fig. 2 – Velocity inlet profile.

Eq. (3) can be cast into the following general form:

$$\frac{d\mathbf{u}_p}{dt} = \frac{1}{\tau_p}(\mathbf{u}\text{-}\mathbf{u}_p) + \mathbf{a} \tag{13}$$

where the term $\mathbf{a}$ includes accelerations due to other forces except drag force.

Integrating the transport Eq. (13) for the path of each particle yields

$$\frac{d\mathbf{x}_p}{dt} = \mathbf{u} \tag{14}$$

where $\mathbf{x}_p$ is the particle position.

With Euler implicit discretization of Eq. (13), we get

$$\mathbf{u}_p^{n+1} = \frac{\mathbf{u}_p^n + \Delta t(a + (\mathbf{u}^n/\tau_p))}{1 + (\Delta t/\tau_p)} \tag{15}$$

The new particle location is computed by a trapezoidal discretization of Eq. (14):

$$x_p^{n+1} = x_p^n + \frac{1}{2}\Delta t(\mathbf{u}_p^n + \mathbf{u}_p^{n+1}) \tag{16}$$

2.3. *Boundary conditions*

The ultrasonic probe surface is set as velocity inlet, and the interface between liquid aluminum and air is pressure outlet. The other boundaries are set as wall. All of the Discrete Phase BC Types are set as reflect. The velocity inlet profile is defined in UDF, which is dependent on time as shown in Fig. 2.

2.4. *Solution procedure*

The SiC nanoparticles are injected at every fluid flow time step with a mass flow rate of 0.014 kg/s in the first second. The distribution of the particle diameters varying from 45 nm to 65 nm follows the Rosin–Rammler expression. Particles are tracked at every time step after the fluid velocity field is solved. Because of the low volume fraction of the discrete phase, one-way coupling is employed, which neglects the effect of the discrete phase on the fluid turbulence.

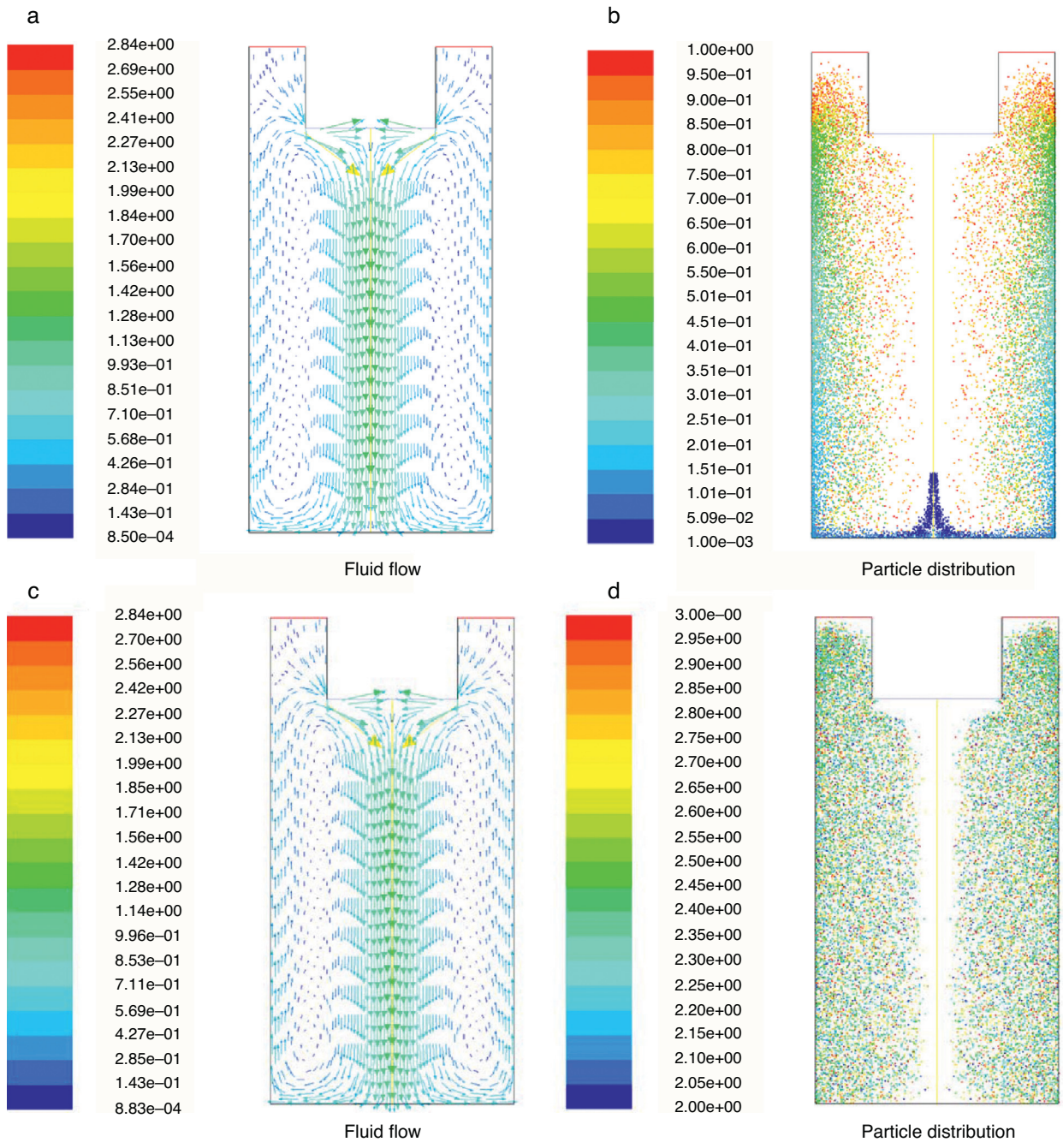

Fig. 3 – Fluid flow and particle distribution after 1s ((a) and (b)) and 3s ((c) and (d)).

3. Simulation results and discussion

Fig. 3 shows the fluid flow (colored by velocity magnitude (in m/s), similarly hereinafter) and particle distribution (colored by particle residence time (in seconds), similarly hereinafter) after 1s and 3s, respectively, when the injection is stopped. It can be seen from Fig. 3a and b that the flow is much stronger at the center of the furnace. Meanwhile, the particles are dispersed well from the bottom to the top, but more particles tend to stay near the wall. The fluid flow and particle distribution after 3s are shown in Fig. 3c and d. It is confirmed that the particles have little effect on the fluid flow because of the one-way coupling, as we can see that the flow field is almost the same as that after 1s. As time goes on after the injection is stopped, the uniformity of the particle distribution becomes even better. However, there are still fewer particles at the center where the flow is stronger, which indicates that the nanoparticles could not disperse well in strong flows. Additionally, the particle distribution stays almost the same henceforth. When the particles are injected from a different position which is about 15 mm beneath the probe, the distributions of the particles after 1s and 3s are shown in Fig. 4.

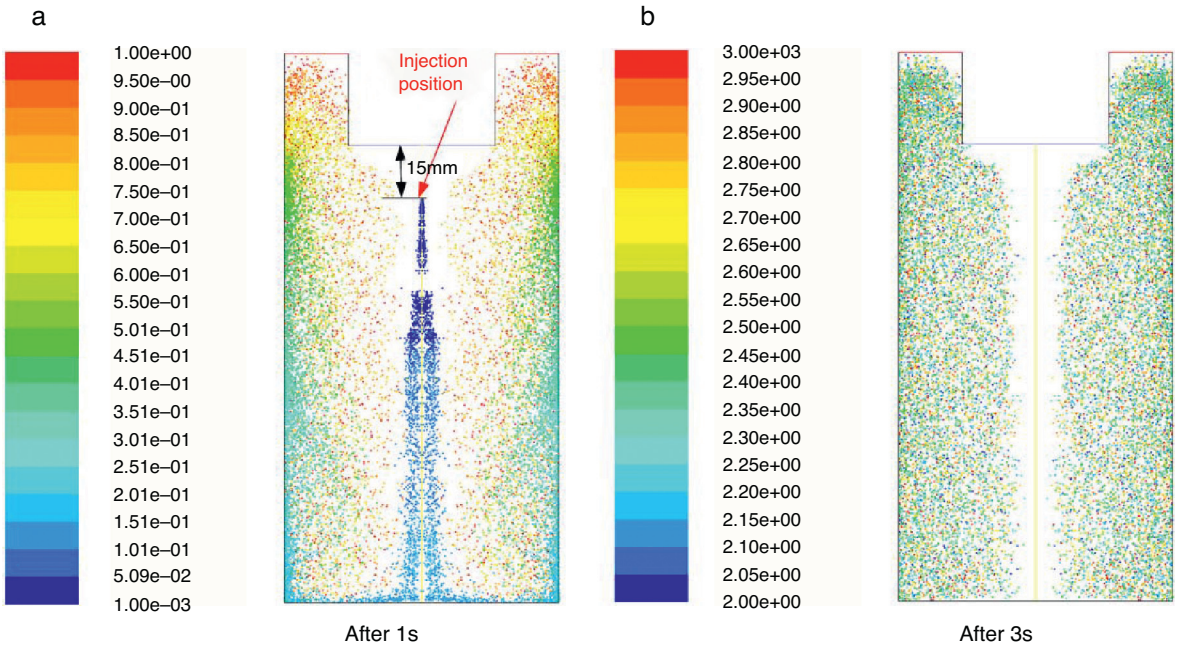

Fig. 4 – Particle distributions after 1s (a) and 3s (b) with a different injection location.

It is obvious that the particles are following the fluid flow. In the beginning, they are carried by the flow in the center to the bottom, and then back to the top near the wall. Nonetheless, after 3s when the distribution becomes stable, it has little difference with that when the particles are injected at the bottom, which demonstrates that the injection position will not affect the final distribution of the SiC nanoparticles.

Fig. 5 presents the fluid flow and particle distribution after 3s when the ultrasonic probe is placed at the bottom of the furnace. The flow pattern is changed due to the gravitational acceleration orientation, thus resulting in a different distribution of the particles. However, the general trend is basically the same, i.e., where the flow is stronger, there are fewer particles, and vice versa.

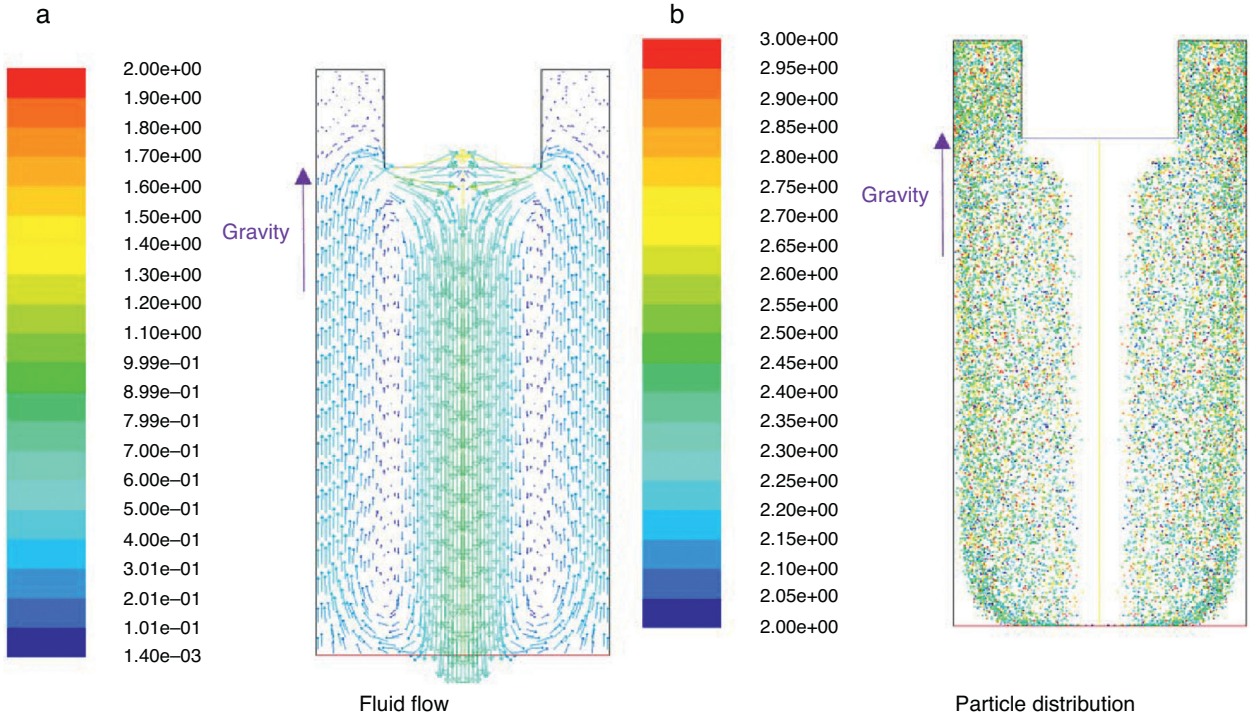

Fig. 5 – Fluid flow and particle distribution after 3s with the ultrasonic probe placed at the bottom of the furnace (gravity vector up).

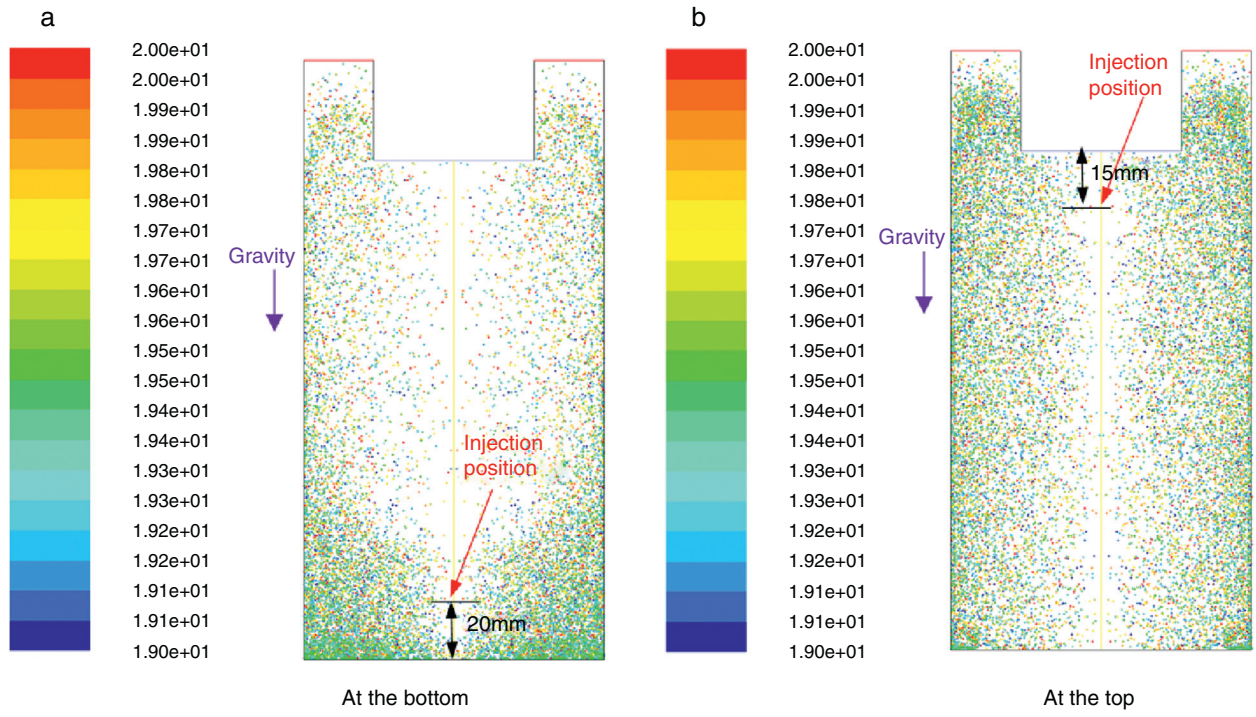

Fig. 6 – Particle distributions after 20s with 2 different injection positions and a weaker flow (gravity vector down).

To investigate the effect of the magnitude of the fluid flow on the dispersion of nanoparticles, the velocity magnitude is changed to be 1/10th of the original one. As the fluid flow is much weaker, the dispersion of the particles is much slower. After 20s, the distributions of the nanoparticles with different injection positions, which are shown in Fig. 6, become almost stable. When the particles are injected at the bottom of the furnace, plenty of them aggregate at the bottom because the fluid flow near the wall is too weak to take them to the top. On the contrary, when they are injected at the top, they can be taken to the bottom by the relatively stronger flow at the middle of the furnace, which results in a much more uniform distribution of the particles.

4. Conclusions and future work

The DDPM model coupled with the $k-\omega$ turbulence model is used to investigate the distribution of SiC nanoparticles with different injection positions and probe locations in the liquid aluminum under the ultrasonic stirring. Several forces acting on a particle including transverse drag force, buoyancy and gravitational force, virtual mass force, pressure gradient force, and lift force are accounted for to predict the trajectory of the particle. The results reveal the following:

1. The particles are dispersed pretty well in the liquid pool except that there are fewer particles at the center of the furnace where the fluid flow is stronger.
2. The injection position will not affect the final distribution of the SiC nanoparticles as long as the flow is strong enough to disperse the particles, otherwise, the injection position will have a significant effect on the distribution of the particles.
3. When the ultrasonic probe is positioned at the bottom of the furnace, i.e., the gravity direction is changed, the nanoparticles have a different distribution due to a new flow pattern.
4. For the fluid flow, there is no doubt that the stronger the flow, the faster the particles are dispersed; however, the uniformity of the fluid flow (and not the intensity of the fluid flow) is crucial to the final distribution of the nanoparticles.

The effects of ultrasonic cavitation and acoustic energy attenuation as well as the furnace wall (lining) trapping of various type of nanoparticles will be determined in a future study.

Conflicts of interest

The authors declare no conflicts of interest.

REFERENCES

[1] Kaczmar JW, Pietrzak K, Wlosinski W. The production and application of metal matrix composite materials. J Mater Process Technol 2000;106:58–67.
[2] Durisinova K, Durisin J, Orolinova M, Durisin M. Effect of particle additions on microstructure evolution of aluminium matrix composite. J Alloys Compd 2012;525:137–42.
[3] William CH. Commercial processing of metal matrix composites. Mater Sci Eng A 1998;244(1):75–9.

[4] Yang Y, Lan J, Li X. Study on bulk aluminum matrix nano-composite fabricated by ultrasonic dispersion of nano-sized SiC particles in molten aluminum alloy. Mater Sci Eng A 2004;380:378–83.
[5] Li X, Yang Y, Weiss D. Ultrasonic cavitation based dispersion of nanoparticles in aluminum melts for solidification processing of bulk aluminum matrix nanocomposite: theoretical study, fabrication and characterization. AFS Transactions. Schaumburg, IL, USA: American Foundry Society; 2007.
[6] Cao G, Konishi H, Li X. Mechanical properties and microstructure of SiC-reinforced Mg-(2,4)Al-1Si nanocomposites fabricated by ultrasonic cavitation based solidification processing. Mater Sci Eng A 2008;486:357–62.
[7] Shin JH, Choi HJ, Cho MK, Bae DH. Effect of the inter face layer on the mechanical behavior of TiO_2 nanoparticle reinforced aluminum matrix composites. J Compos Mater 2014;48(1):99–106.
[8] Dikici B, Gavgali M, Bedir. Synthesis of *in situ* TiC nanoparticles in liquid aluminum: the effect of sintering temperature. J Compos Mater 2010;45(8):895–900.
[9] El-Daly AA, Abdelhameed M, Hashish M, Daoush WM. Fabrication of silicon carbide reinforced aluminum matrix nanocomposites and characterization of its mechanical properties using non-destructive technique. Mater Sci Eng A 2013;559:384–93.
[10] Jiang X, Galano M, Audebert F. Extrusion textures in Al, 6061 alloy and 6061/SiC_p nanocomposites. Mater Charact 2014;88:111–8.
[11] Shin JH, Bae DH. Effect of the TiO_2 nanoparticle size on the decomposition behaviors in aluminum matrix composites. Mater Chem Phys 2014;143:1423–30.
[12] Borgohain C, Acharyya K, Sarma S, Senapati KK, Sarma KC, Phukan P. A new aluminum-based metal matrix composite reinforced with cobalt ferrite magnetic nanoparticle. J Mater Sci 2013;48:162–71.
[13] Sautter FK. Electrodeposition of dispersion-hardened Nickel–Al_2O_3 alloys. J Electrochem Soc 1963;110:557.
[14] Fluent 6.3. User's guide manual fluent inc. and ansys's fluent; 2006 http://ansys.com/